Characterising the short-term habituation of event-related evoked potentials

Flavia Mancini[1, 2,*], Alessia Pepe[3], Giulia Di Stefano[3],
André Mouraux[4], Gian Domenico Iannetti[1]

[1]*Department of Neuroscience, Physiology and Pharmacology, University College London, London, UK*
[2]*Computational and Biological Learning Lab, Department of Engineering, University of Cambridge, Cambridge, UK*
[3]*Department of Neurological Sciences, University of Rome 'La Sapienza', Rome, IT*
[4]*Institute of Neuroscience, Université Catholique de Louvain, Brussels BE*

* *Corresponding author:*
Flavia Mancini
University of Cambridge
Department of Engineering, Computational and Biological Learning Lab
Trumpington Street, Cambridge, CB2 1PZ
fm456@cam.ac.uk

Abstract

Fast-rising sensory events evoke a series of functionally heterogeneous event-related potentials (ERPs), which reflect the activity of both modality-specific and supramodal cortical generators overlapping in time and space. When stimuli are delivered at long and variable intervals (e.g., 10-15 seconds), supramodal components appear as a large negative-positive biphasic deflection maximal at the scalp vertex (vertex wave) and dominate over modality-specific components. Stimulus repetition at 1 Hz induces a strong habituation of these supramodal components, which largely reflect stimulus saliency and behavioural relevance. In contrast, the effect of stimulus repetition on lateralized modality-specific components has been less explored, and the few existing results are inconsistent. To comprehensively characterize how the different ERP waves habituate over time, we recorded the ERPs elicited by 60 identical somatosensory stimuli (activating either non-nociceptive Aβ or nociceptive Aδ afferents), delivered at 1 Hz to healthy human participants. We show that the well-described spatiotemporal sequence of modality-specific and supramodal ERP components elicited by the first stimulus of the series is largely preserved in the smaller-amplitude, habituated response elicited by the last stimuli of the series. We also modelled the single-trial amplitude of both the lateralised modality-specific wave (N1) and the centrally-distributed vertex waves (N2 and P2) elicited by the 60 stimuli. The vertex waves decayed monotonically, with a largest drop of response magnitude at the first stimulus repetition followed by much smaller decreases in subsequent repetitions. In contrast, the lateralised somatosensory waves did not habituate consistently across the block.

New & Noteworthy

We characterized the decay of event-related potentials (ERPs) elicited by identical fast-rising stimuli repeated at 1Hz. Our observations indicate that, although response amplitude is reduced by stimulus repetition, both non-habituated and habituated ERPs are obligatory contributed by both modality-specific lateralized components and supramodal vertex components. Only supramodal components decay sharply at the first stimulus repetition, whereas modality-specific components do not. This suggests that modality-specific and supramodal components of the ERP habituate to stimulus repetition at different timescales.

Introduction

Sudden sensory events evoke a series of transient responses in the ongoing electrocortical activity (event-related potentials, ERPs). ERPs are functionally heterogeneous and reflect the activity of distinct cortical generators overlapping in time and space (Sutton et al., 1965). Since these generators include both primary sensory and associative cortical areas, the scalp distribution of the ERPs elicited by stimuli of different modalities partly differs depending on the modality of the sensory input. However, when elicited by isolated and intense fast-rising stimuli, the activity of generators reflecting supramodal neural activities dominates over modality-specific activities (Liang et al., 2010). The scalp distribution of the electroencephalogram (EEG) signal reflecting supramodal generators is virtually identical regardless of the modality of the eliciting stimulus: it consists in a biphasic negative-positive deflection widespread over the scalp and maximal at the vertex – often referred to as 'vertex wave' or 'vertex potential' (Bancaud et al., 1953).

The vertex wave amplitude is maximal when fast-rising stimuli are presented using large and variable inter-stimulus intervals of several seconds (Mouraux and Iannetti, 2009; Huang et al., 2013), or when the stimulus reflects behaviourally relevant changes within a regular series of otherwise identical stimuli (Snyder and Hillyard, 1976; Valentini et al., 2011; Ronga et al., 2013). In contrast, when identical stimuli are monotonously repeated at short and regular intervals (e.g., 0.5 or 1 Hz), the vertex wave amplitude strongly decays (Jasper and Sharpless, 1956; Ritter et al., 1968; Davis et al., 1972; Mouraux and Iannetti, 2009; Liang et al., 2010; Wang et al., 2010). For this reason, the vertex wave has been suggested to be related to the detection and immediate reaction to behaviourally-relevant, sudden events (Sutton et al., 1965; Mouraux and Iannetti, 2009), a hypothesis also supported by preliminary behavioural evidence (Wessel and Aron, 2013; Moayedi et al., 2016). Although the decay of the vertex wave due to repeated stimulation at different stimulation frequencies has been described (Fruhstorfer et al., 1970; Greffrath et al., 2007), a formal characterization of how the different constituent components of the ERP habituate over time is still missing. This is particularly important considering that previous studies suggested that neural activity in different cortical regions may adapt to repeated stimulation at different timescales: for instance, neural activity in associative regions elicited by trains of innocuous, somatosensory stimuli decays faster than neural activity in sensory cortices (Forss et al., 2001; Venkatesan et al., 2014). However, these results may not generalise to responses elicited by noxious somatosensory stimuli: a previous study has suggested that the repetition of electrical nociceptive stimuli at 1 Hz for 1 minute suppresses evoked responses originating in primary somatosensory cortex (Mouraux et al., 2013).

Therefore, our primary objective was to describe the short-term habituation of the different constituents of somatosensory ERPs: both the large supramodal vertex waves and the smaller modality-specific lateralised waves. ERPs elicited by transcutaneous electrical stimulation of nerve trunks provide an excellent model to achieve this objective. Indeed, this stimulation activates directly all large-diameter Aβ somatosensory afferents, thus resulting in a synchronous volley that elicits cortical responses with a large signal-to-noise ratio. Furthermore, somatosensory ERPs are well characterised in terms of deflections, topographies and underlying generators (Treede et al., 1988; Hu et al., 2014b).

We recorded EEG while delivering trains of 60 identical Aβ stimuli at 1 Hz. We characterized the ERP habituation in three complementary ways. First, we compared the ERP amplitudes between the first

and last stimuli of the block. Second, we statistically assessed the presence of the main response components in both the non-habituated ERP (i.e. the ERP elicited by the first stimulus of a series) and the habituated ERP (i.e. the ERP elicited by later stimuli that elicit a stable, habituated response). The rationale for this decision was the consistent observation that the amplitude of the main ERP waves (i.e., vertex waves) decays only minimally after the first few stimulus repetitions (Ritter et al., 1968; Fruhstorfer et al., 1969; Fruhstorfer et al., 1970; Fruhstorfer, 1971; Greffrath et al., 2007; Mouraux et al., 2013), a finding corroborated by the present results (Figures 1-4). Third, we fitted a number of functions derived from previous studies (Fruhstorfer et al., 1970; Greffrath et al., 2007), to model the time-profile of the decay of the supramodal negative and positive vertex waves. To cross-validate and generalise our findings across different sensory pathways, we replicated the experiment in a separate group of healthy participants, using radiant-heat stimuli that selectively activate skin nociceptors and elicit sensations of Aδ-mediated pinprick pain.

Methods

Participants

Thirty-two healthy subjects (14 women) aged 19–31 years (mean ± SD: 23.6 ± 3.9) participated in the study, after having given written informed consent. All experimental procedures were approved by the ethics committee of University College London (2492/001).

Transcutaneous electrical stimulation of Aβ fibers

Innocuous stimulation of Aβ afferents consisted of square-wave pulses (100 μs duration), generated by a constant current stimulator (DS7A, Digitimer, UK). Stimuli were delivered through a bipolar electrode placed above the superficial radial nerve, and elicited a paresthetic sensation in the corresponding innervation territory. Aβ detection thresholds were identified using the method of ascending staircases, on the right hand. The detection threshold was defined as the average of the lowest stimulus energy eliciting a sensation in 3 consecutive trials. Electrical stimuli were delivered at approximately 300% of each individual's Aβ detection threshold. Stimulus intensity was slightly adjusted to elicit sensations of comparable intensities on the left and right hands (mean ± SD, 17.4 ± 11.4 mA) and to make sure that the elicited sensation was never painful.

Cutaneous laser stimulation of Aδ and C fibers

Nociceptive stimuli were radiant heat pulses generated by an infrared neodymium:yttrium-aluminum-perovskite laser with a wavelength of 1.34 μm (Nd:YAP; Electronical Engineering, Italy). At this wavelength, laser pulses excite Aδ and C nociceptive free nerve endings in the epidermis directly and selectively, i.e. without coactivating touch-related Aβ fibers in the dermis (Bromm and Treede, 1984; Baumgartner et al., 2005; Mancini et al., 2014). The duration of each laser pulse was 4 ms.

Laser stimuli were delivered within a squared skin area (4 x 4 cm) centered on the dorsum of the hand, encompassing the area in which the stimulation of Aβ afferents elicited the paraesthesia. The laser

beam was transmitted through an optic fiber, and its diameter at target site was set at ~6 mm by focusing lenses. A visible He–Ne laser pointed to the stimulated area.

The method of ascending staircases used for identifying the detection threshold of Aβ stimuli was also used to identify the detection threshold of Aδ stimuli. For the EEG recordings, the stimulus energy was clearly above the activation threshold of Aδ fibers (0.53 ± 0.06 J/mm^2). This stimulus energy elicited intense but tolerable pinprick pain sensations, of comparable intensities on the right and left hands. Because variations in baseline skin temperature may modulate the intensity of the afferent nociceptive input (Iannetti et al., 2004), an infrared thermometer was used to ensure that the hand temperature varied no more than 1°C across blocks. To avoid receptor fatigue or sensitization, the laser beam was displaced after each stimulus by ~1 cm within the predefined stimulated area.

Experimental procedure

Participants sat comfortably with their hands resting on a table in front of them. They were instructed to focus their attention on the stimuli, and fixate a yellow circular target (diameter: 1 cm) placed in front of them at a distance of approximately 60 cm from their face. A black curtain blocked the view of the hands. Throughout the experiment, white noise was played through headphones, to mask any sound associated with the either type of somatosensory stimulation.

The experiment was performed on 32 participants, divided in two groups of 16 participants. One group received electrical stimuli, and the other group received laser stimuli, using an identical procedure. Each participant received the somatosensory stimuli in 10 blocks, separated by a 5-minute interval, during which participants were allowed to rest. Each block consisted of 60 somatosensory stimuli delivered at 1 Hz: thus, each block lasted 1 minute. In each block, stimuli were delivered either to the right hand or to the left hand. Right- and left-hand blocks were alternated. The order of blocks was balanced across participants; half of the subjects started with a right-hand block, and the other half started with a left-hand block. At the end of each block, participants were asked to provide an average rating of perceived stimulus intensity, using a numerical scale ranging from 0 ("no sensation") to 10 ("most intense sensation"). This was done to ensure that the perceived intensity of the stimuli was similar across blocks (rating variability (SD) across blocks: electrical stimuli, 0.2 ± 0.2; laser stimuli: 0.3 ± 0.4).

Electrophysiological recordings

EEG was recorded using 30 Ag–AgCl electrodes placed on the scalp according to the International 10-20 system (Electro-Cap International; USA), using the nose as reference. Electrode positions were 'Fp1', 'Fpz', 'Fp2', 'F7', 'F3', 'Fz', 'F4', 'F8', 'T3', 'C3', 'Cz', 'C4', 'T4', 'T5', 'P3', 'Pz', 'P4', 'T6', 'O1', 'Oz', 'O2', 'FCz', 'FC4', 'FC3', 'Cp3', 'Cp4'. Eye movements and blinks were recorded from the right *orbicularis oculi* muscle, using 2 surface electrodes. The active electrode was placed below the lower eyelid, and the reference electrode a few centimetres laterally to the outer canthus. Signals were amplified and digitized using a sampling rate of 1,024 Hz (SD32; Micromed, Italy).

EEG analysis

1. Preprocessing. EEG data were preprocessed and analyzed using Letswave 6 (http://www.nocions.org/letswave/) and EEGLAB (https://sccn.ucsd.edu/eeglab/). Continuous EEG data were band-pass filtered from 0.5 to 30 Hz using a Butterworth filter, segmented into epochs using a time window ranging from -0.2 to 0.8 sec relative to the onset of each stimulus, and baseline corrected using the interval from -0.2 to 0 sec as reference. Trials contaminated by large artefacts (<10% in each block) were removed. Eye blinks and movements were corrected using a validated method based on unconstrained Independent Component Analysis ("runica" algorithm of EEGLAB). In all datasets, independent components related to eye movements showed a large EOG channel contribution and a frontal scalp distribution. To allow averaging across blocks while preserving the possibility of detecting lateralized EEG activity, scalp electrodes were flipped along the medio-lateral axis for all signals recorded in response to left hand stimulation.

2. Statistical assessment of ERP components. To assess decay of the ERP response, we first statistically compared the response amplitude at the beginning and at the end of the block (note that a more formal quantification of the response habituation was provided by the modelling analyses described in the next section). We performed four paired-sample t-tests to compare the amplitude of the response to the 1st stimulus vs the 2nd stimulus, and to the 1st vs the last (60th) stimulus. We also compared the amplitude of the ERPs elicited by the 2nd vs 3rd stimulus, and 59th vs 60th stimulus. All t-tests were performed for each time point of the ERP timecourse, and for all electrodes. Thus, this analysis yielded a scalp distribution of t-values across time, for each modality. To account for multiple comparisons, significant time points ($p < 0.05$) were clustered based on their temporal adjacency (cluster-level statistical analysis). For each cluster, we calculated the pseudo-*t* statistic of the two conditions, estimated its distribution by permutation testing (1000 times), and generated the bootstrap *p* values for testing the null hypothesis that there were no differences in signal amplitude (Maris and Oostenveld, 2007). This procedure identified the clusters in which the responses in two given conditions were significantly different.

Second, we assessed the consistency of stimulus-evoked modulations of EEG amplitude across time, to statistically evaluate whether EEG deflections in the post-stimulus time window (from 0 to +0.8 s) was significantly greater than baseline. Specifically, we performed a one-sample t-test against zero (i.e. against baseline) for each electrode and time point of the entire baseline-corrected waveform, using cluster-level permutation testing. This analysis yielded a scalp distribution of t-values across time, and was performed separately on the non-habituated ERP and on the habituated ERP of each modality. The non-habituated ERP was derived by averaging all the responses elicited by the 1st stimulus of all blocks. The habituated ERP was derived by averaging the responses elicited by the 6th to the 60th stimuli of all blocks. The decision of using these responses elicited by stimuli 6th to 60th as a proxy of the habituated ERP was based on the observation that the amplitude of the main ERP waves decays only minimally after the first 5 stimulus repetitions, as observed here (Figure 1-2, 4) and previously described (Fruhstorfer et al., 1970; Greffrath et al., 2007). Figures 1, 2, and 4 show how the amplitude of the ERPs was consistently habituated after the first few stimulus repetitions.

3. Modelling the within-block decay of the vertex waves. We tested whether the amplitude of the N2 and P2 vertex waves and of the N1 lateralized wave evoked by Aβ and Aδ stimuli decayed following different functions derived from previous studies (Fruhstorfer et al., 1970; Greffrath et al., 2007). In each participant, we first averaged each of the 60 ERP responses across the 10 recording blocks, and thus obtained 60 average ERP waveforms: one for each of the 60 trials. Then, we averaged across

participants and obtained 60 group-level averages. On these averages, we measured the latency and amplitude values of the 60 N2 and P2 peaks at Cz (referenced to the nose) and of the 60 N1 peaks at Cc (referenced to Fz), using a validated procedure based on multiple linear regression (Hu et al., 2010; Hu et al., 2011). Finally, we modelled the decay of the N1, N2 and P2 peak amplitudes across the 60 trials, using three different equations:

(1) $y = a + \frac{b}{x}$

(2) $y = a + \frac{b}{x^c}$

(3) $y = a + e^{-bx}$

where y is the peak amplitude of each given ERP wave, x is the trial number (from 1 to 60), e is the Euler constant, and a, b, c are the parameters to be estimated using a least squares method. Model fitting was performed on the signal averaged across subjects, rather than on each individual subject, because the signal-to-noise ratio of the habituated N1 wave is very low at single-trial and single-subject levels, making the extraction of N1 peaks not always reliable (Hu et al., 2010). We tested these specific models of ERP decay given the previous evidence that the vertex wave decays sharply at the first stimulus repetition (Fruhstorfer et al., 1970; Greffrath et al., 2007; Mouraux and Iannetti, 2009; Valentini et al., 2011; Ronga et al., 2013). No constraints were set on the parameters to be estimated. The decay of the N2 and P2 vertex components was modelled separately, because these waves can be independently modulated (Legrain et al., 2002; Hatem et al., 2007). To compare which model best fitted the data, we calculated the adjusted r^2 and the Akaike information criterion of each model, corrected for low sample size (AICc). The AIC is a relative estimate of the information lost in a given model, and it allows a fair comparison between non-linear models of different complexity, i.e. even when they have a different number of parameters. The lower the AIC, the better the model represents the measured data. From the difference in AICc values, we calculated the probability that each model was correct, with the probabilities summing to 100% (Burnham and Anderson, 2002). Finally, we tested for equal variance of the residuals using the 'test for appropriate weighting', as implemented in Prism GraphPad 7.0.

Results

Response waveforms and topographies

Group-average ERPs elicited by Aβ and Aδ stimuli are shown in Figures 1, 2 and 3. As expected, the latency of Aδ-ERPs was longer than the latency of Aβ-ERPs, because Aδ fibers are thinly myelinated and thus have slower conduction velocity than large-myelinated Aβ fibers (Mountcastle, 2005).

Figure 1 shows that the amplitude decay of the negative and positive vertex waves (N2 and P2) elicited by the 60 repeated somatosensory stimuli. Both N2 and P2 dramatically decreased after the very first stimulus repetition (trial #1 vs. #2), in both stimulus modalities. In contrast, no wave except the Aβ-P2 further decreased at the second stimulus repetition (trial #2 vs. #3) (Figure 1). Figure 3 demonstrates that, both in the non-habituated response (trial #1) and in the habituated response (average of trials #6-60), the N2 and P2 waves were greater than baseline. Not only they survived 1-minute of repeated

stimulation, but clearly dominated the majority of the ERP responses (see also Supplementary Results and Figures S1-S2).

Figure 2 shows the lack of any significant amplitude decay of the lateralized waves (N1 and P4) elicited by the 60 repeated somatosensory stimuli. In both stimulus modalities, these waves were much smaller than the vertex waves, as expected (Valentini et al., 2012; Hu et al., 2014a). Paired t-tests showed no consistent habituation of the N1 and P4 waves at the first repetition of either Aβ or Aδ stimuli (trial #1 vs #2), and no significant habituation of any lateralised wave between the first and last stimulus of the block (trial #1 vs #60; Figure 2). Importantly, albeit small in amplitude, both the early N1 and the late P4 lateralized waves elicited in trials 1 and 6-60 were nevertheless consistently greater than baseline, as demonstrated by the point-by-point *t*-tests reported in Figure 3. The peaks of the N1 and P4 waves elicited in trials 1 and 6-60 had maximal spatial distribution over the central electrodes in the hemisphere contralateral to hand stimulation (Figure 3), as shown in previous studies (Hu et al., 2014a; Mancini et al., 2015).

Modelling the decay of the vertex wave elicited by stimuli repeated at 1 Hz

Figure 4 displays the fit of the three models of ERP decay we tested on the average peaks of the N2, P2, and N1 waves. The same model best predicted the decay of the vertex N2 and P2 waves elicited by Aβ and Aδ stimuli. This winning model was equation #2, and the decay of the four peaks was described as follows:

$$\text{A}\beta\ \text{N2} = -4.22 - \frac{19.37}{x^{1.46}}$$

$$\text{A}\beta\ \text{P2} = 9.12 + \frac{14.52}{x^{1.35}}$$

$$\text{A}\delta\ \text{N2} = -5.01 - \frac{14.03}{x^{2.05}}$$

$$\text{A}\delta\ \text{P2} = 8.34 + \frac{14.37}{x^{2.51}}$$

where x is the trial number. The AICc and the adjusted r^2 values for all models are reported in Table I: the fitting of equation #2 gave the lowest AICc and the highest adjusted r^2 values. Furthermore, the residuals of the winning models were homoscedastic ($p > 0.999$). In qualitative terms, winning model #2 indicates that the amplitude of the examined peaks decays monotonically, with a fastest and sharpest drop of response magnitude at the first stimulus repetition, followed by much smaller decreases in the subsequent repetitions.

The fitting of the decay of the Aβ-N1 and Aδ-N1 waves was rather poor, possibly because of the low signal-to-noise ration at single-trial level. The winning model was again equation #2, although the coefficients of determination were low (adjusted $r^2 = 0.28$ for the Aβ-N1, and 0.33 for the Aδ-N1). This indicates that a large proportion of the variance of the data was not described by the winning model. Hence, none of the models that we chose *a priori* gave a sufficiently accurate description of the data. Therefore, we explored *post hoc* the fitting of other models (linear, power, sigmoidal, logistic, 1-6 degrees polynomial, and Fourier functions), but also these models poorly explained the variability of

Aβ-N1 and Aδ-N1 peak amplitude across stimulus repetitions (all adjusted $r^2 < \pm 0.1$). Thus, we found no consistent and reliable evidence of habituation of the N1 across the block.

Discussion

In this study, we characterised the habituation of modality-specific and supramodal ERP components elicited by 60 identical somatosensory stimuli (activating either Aβ non-nociceptive, or Aδ nociceptive primary afferents) delivered at 1 Hz. Although the response amplitude was clearly reduced, the spatiotemporal sequence of the ERP waves was overall preserved in the habituated response (Figures 3, S1, S2). This was substantiated by point-by-point statistical analysis: both somatosensory-specific and supramodal components typically observed in the ERP elicited by sporadic and unpredictable stimuli (Liang et al., 2010; Hu et al., 2014a; Mancini et al., 2015) also contributed to the ERP elicited by frequent and predictable stimuli. Furthermore, our results indicate that the supramodal ERP components habituate dramatically at the very first stimulus repetition, whereas early somatosensory-specific ERP components do not decay consistently neither at the first stimulus repetition nor across 60 trials.

Effect of stimulus repetition on supramodal ERP responses

The negative-positive vertex wave (VW) is the largest component of the EEG response elicited by sudden sensory stimuli. Its high signal-to-noise ratio makes the VW amplitude measurable in single trials, even when the response is habituated by stimulus repetition. Therefore, we were able to estimate the amplitude of the negative (N2) and positive (P2) vertex waves for each of the 60 ERPs (Figure 4). The decay of the negative and positive peaks was best modelled as follows:

$$y = a + \frac{b}{x^c}$$

where y is the peak amplitude of the N2 or P2 wave, x is the trial number, and a, b, c are the estimated parameters. This indicates that the amplitude of both vertex waves decays monotonically, with a largest, transient drop of response magnitude at the first stimulus repetition, followed by much smaller decreases in subsequent repetitions. This observation is further supported by point-by-point t-tests displayed in Figure 1.

Converging evidence indicates that stimuli of virtually all sensory modalities can elicit a VW, provided that they are salient enough (Liang et al., 2010). It is therefore not surprising that the VW elicited by auditory stimuli repeated at 1-Hz decays following a function similar to the one observed here for somatosensory stimuli (Fruhstorfer et al., 1970). Even when considering experimental observations that did not formally model the response habituation, the maximum decrease in VW amplitude consistently occurs at the first stimulus repetition, for auditory (Ritter et al., 1968; Fruhstorfer et al., 1970), somatosensory (Larsson, 1956; Fruhstorfer, 1971; Iannetti et al., 2008; Wang et al., 2010; Valentini et al., 2011; Ronga et al., 2013) and visual stimuli (Courchesne et al., 1975; Wastell and Kleinman, 1980). The similarity of the decay of the VW elicited by Aβ and Aδ stimuli (Figures 1, 3, 4) further supports the multimodal nature of the neural generators of these signals (Mouraux and Iannetti, 2009). The mechanisms underlying such sharp reduction of response amplitude at the first stimulus repetition are likely to be similar across sensory systems.

Before discussing the contribution of the present results in elucidating the functional significance of the VW, it is important to highlight the empirical evidence that the observed response habituation is not due to neural refractoriness of afferent neurons or to fatigue of primary receptors. A previous study recorded ERPs elicited by pairs of nociceptive stimuli delivered at short intervals, which could be either identical or variable across the block (Wang et al., 2010). Only when the inter-stimulus interval was *constant* across the block, the VWs elicited by the second stimulus were reduced in amplitude. The peak amplitude of the VWs elicited by the second stimulus was instead as large as the VWs elicited by the first stimulus when the inter-stimulus interval was *variable*, indicating that neither neural refractoriness nor fatigue can easily explain the sharp response decay to stimulus repetition.

Furthermore, if the sharp response habituation at the first stimulus repetition was determined by fatigue of primary sensory receptors, we would have observed different decay profiles for stimuli delivered in varying vs constant spatial locations. Indeed, the VW elicited by contact heat stimuli at long and variable intervals (8-10 seconds) decays much faster if the second stimulus is delivered at the same spatial location of the first (Greffrath et al., 2007). Instead, we observed remarkably similar patterns of ERP decay for both Aδ laser stimuli delivered at different spatial locations and Aβ electrical stimuli delivered in the same skin region. Additionally, electrical stimuli activate directly the axons in the nerve trunk, bypassing the receptor, further ruling out receptor fatigue as explanation for the Aβ-ERP habituation. Receptor fatigue might still contribute to the slow decrease in ERP magnitude observed across dozens of stimulus repetitions of laser stimuli (Greffrath et al., 2007), but certainly not to the dramatic reduction of ERP amplitude we observed after one single stimulus repetition.

The physiological significance of the VW remains to be properly understood. However, there is evidence that this large electrocortical response reflects neural activities related to the detection of salient environmental events (Jasper and Sharpless, 1956; Mouraux and Iannetti, 2009) and execution of defensive movements (Moayedi et al., 2015). The detection of salient events relies on a hierarchical set of rules that consider both their probability of occurrence and their defining basic features (Legrain et al., 2002; Wang et al., 2010; Valentini et al., 2011; Ronga et al., 2013; Moayedi et al., 2016). The present results are informative with respect to this functional framework. Indeed, stimulus repetition did not abolish the VW elicited by either Aβ or Aδ stimuli, although it reduced its amplitude already after the first stimulus repetition. Therefore, even when stimulus saliency is reduced by contextual factors, there is a residual activity of the VW generators, only minimally reduced after the first few stimulus repetitions (Figures 1, 3, S1, S2). These findings point towards the existence of an obligatory VW activity triggered by any sudden and detectable change in the environment, even when contextual modulations minimize its behavioural relevance.

Extensive evidence from cell physiology indicates that neural habituation to repeated stimuli arises from alterations of synaptic excitability. Even the simple gill-withdrawal reflex in Aplysia dramatically habituates at the first stimulus repetition (Byrne et al., 1978), due to a decreased drive from the sensory neurons onto follower motor neurons (Castellucci et al., 1970; Carew and Kandel, 1973). The temporal profile of this short-term habituation follows a fast decay function (Carew and Kandel, 1973), strikingly similar to that observed in this and other studies on the habituation of electrocortical responses in humans (Fruhstorfer et al., 1970; Greffrath et al., 2007). These synaptic changes have been interpreted as a hallmark of learning, and are central to the ability of the nervous system to adapt to environmental events (Carew and Kandel, 1973). Interpreting the decay of neural responses as functionally relevant for

learning is not in contradiction with attentional interpretations: stimuli that are learned and recognized are likely to require less attentional resources than novel stimuli, and stimuli that need to be learned are typically more salient.

Effect of stimulus repetition on somatosensory lateralized responses

In somatosensory ERPs, the VW is both preceded and followed by other deflections of smaller amplitude. These have a topographical distribution maximal over centro-parietal electrodes in the hemisphere contralateral to hand stimulation. The earliest negative wave is usually referred to as N1 (Valentini et al., 2012) and the latest positive waveform of somatosensory ERPs is referred to as P4 (Hu et al., 2014a; Mancini et al., 2015). Whereas the P4 has only been recently identified and its significance is not yet understood, the N1 has been described repeatedly in a large body of studies (Treede et al., 1988; Spiegel et al., 1996; Garcia-Larrea et al., 2003; Lee et al., 2009; Hu et al., 2014a; Mancini et al., 2015), and reflect somatosensory-specific neural activities more obligatorily related to the incoming afferent input (Lee et al., 2009; Liang et al., 2010). Both N1 and P4 are likely to originate in the primary somatosensory cortex (Treede et al., 1988; Valentini et al., 2012; Hu et al., 2014a).

We showed that these modality-specific N1 and P4 responses are detectable not only in the response to the first stimulus, but also in the habituated ERP response, as supported by the statistical assessment of the scalp distribution of the ERP response elicited by both the first and the last stimuli of the series (Figure 3). This is important, given that a previous study using trains of intra-epidermal electrical shocks at 1 Hz failed to observe any lateralized response (Mouraux et al., 2013). It is difficult to reconcile these two different observations, and we can only speculate about why that previous experiment failed to detect lateralised responses in the habituated response. One possibility is that intra-epidermal electrical stimulation causes a stronger peripheral and perceptual habituation, more significant than for radiant heat stimulation (Mouraux et al., 2010).

Finally, our study does not provide evidence of any consistent effect of stimulus repetition on the amplitude of somatosensory-specific waves (Figures 2 and 4). This might simply be due to the fact that N1 and P4 waves have small amplitudes and poor signal-to-noise ratio at single trial level (Hu et al., 2010). However, a previous MEG study has also reported that neural activity originating from primary somatosensory cortex is more resilient to stimulus repetition (2-Hz pneumatic stimulation of the fingers and face): in other words, it decays to a less extent and more slowly than neural activity in higher-order cortical regions, such as the posterior parietal cortex (Venkatesan et al., 2014).

In conclusion, our results provide a functional characterization of the decay of the different ERP components when identical somatosensory stimuli are repeated at 1Hz. Fast-rising stimuli elicit ERPs obligatory contributed by both modality-specific and supramodal neural activities, even when stimulus repetitions minimize stimulus relevance. This indicates a fundamental and compulsory property of the nervous system: its sensitivity to respond to sudden changes in the environment with a transient synchronization of thalamocortical activity that manifests itself as widespread brain potentials detectable in the human EEG. The large supramodal vertex waves decay sharply at the first stimulus repetition, whereas smaller modality-specific waves do not appear to habituate consistently across stimulus repetitions. These results suggests that modality-specific and supramodal components of the ERP habituate to stimulus repetition at different timescales.

Figure captions

Figure 1. *Habituation of supramodal vertex waves (N2, P2) elicited by repeated Aβ (left panel) and Aδ (right panel) stimuli.* The figure shows the ERPs elicited by 60 stimuli delivered at 1 Hz, at electrode Cz referenced to the nose (vertex waves). The responses to both the first five stimuli and the last five stimuli are enlarged and presented super-imposed, to facilitate visual comparison. To assess possible habituation effects, we used paired-sample *t*-tests with cluster-based permutation testing to compare the amplitude of the ERP elicited in trial #1 vs #2, trial #1 vs #60, trial #2 vs #3, and trial #59 vs #60, for each time point of the waveform and scalp electrode. Point-by-point *t* values are shown on the bottom panels of the figure. Time intervals during which the ERP waves were significantly different at $p < 0.05$ are highlighted in orange.

Figure 2. *Habituation of lateralized somatosensory waves (N1, P4) elicited by repeated Aβ (left panel) and Aδ (right panel) stimuli.* The figure shows the ERPs elicited by 60 stimuli delivered at 1 Hz, at electrode Cc referenced to Fz. The responses to both the first five stimuli and the last five stimuli are enlarged and presented super-imposed, to facilitate visual comparison. To assess possible habituation effects, we used paired-sample *t*-tests with cluster-based permutation testing to compare the amplitude of the ERP elicited in trial #1 vs #2, trial #1 vs #60, trial #2 vs #3, and trial #59 vs #60, for each time point of the waveform and scalp electrode. Point-by-point *t* values are shown on the bottom panels of the figure. Time intervals during which the ERP waves were significantly different at $p < 0.05$ are highlighted in orange.

Figure 3. *Habituation of supramodal vertex waves (N2, P2) and lateralized responses (N1, P4) elicited by Aβ (top panel) and Aδ (right panel) somatosensory stimuli.* Displayed signals show group-level ERPs recorded from the vertex (Cz vs nose) and from the central electrode contralateral to the stimulated hand (Cc vs Fz), elicited by the first stimulus in a series (non-habituated response) and by the average of trials #6-60 (habituated response). Scalp topographies (signals referenced to the nose) are displayed at the peak latency of the N1, N2, P2, and P4 waves, in all conditions. To assess the consistency of stimulus-evoked modulations of ERP amplitude across time, we performed a one-sample *t*-test against zero (i.e. against baseline) with cluster-based permutation testing, for each electrode and time point of the waveform. Point-by-point *t* values are shown below the ERPs. Time intervals during which the ERP waves were significantly different than 0 in the N1, N2, P2, and P4 time windows are highlighted in orange.

Figure 4. *Modelling the decay of the vertex waves (N2, P2) and lateralized waves (N1) elicited by repeated Aβ (left panels) and Aδ (right panels) stimuli.* The average peak amplitudes of the N2 (blue circles), P2 (yellow circles) and N1 waves (lilac circles) are displayed for each of the 60 trials. The function that best fit the decay of the N2 and P2 amplitudes (equation #2 in the main text, here indicated by the arrow) is displayed with a black dashed line.

Acknowledgments

FM and GDI were supported by a Wellcome Trust Strategic Award (COLL JLARAXR). GDI is additionally supported by a ERC Consolidator Grant (PAINSTRAT) and by the Medical Research Council. AM is supported by an ERC Starting Grant (PROBING-PAIN). The authors declare no competing financial interests.

References

Bancaud J, Bloch V, Paillard J (1953) [Encephalography; a study of the potentials evoked in man on the level with the vertex]. Rev Neurol (Paris) 89:399-418.

Baumgartner U, Cruccu G, Iannetti GD, Treede RD (2005) Laser guns and hot plates. PAIN 116:1-3.

Bromm B, Treede RD (1984) Nerve fibre discharges, cerebral potentials and sensations induced by CO2 laser stimulation. Hum Neurobiol 3:33-40.

Burnham KP, Anderson DR (2002) Model Selection and Multimodel Inference, 2nd Edition: Springer-Verlag.

Byrne JH, Castellucci VF, Kandel ER (1978) Contribution of individual mechanoreceptor sensory neurons to defensive gill-withdrawal reflex in Aplysia. J Neurophysiol 41:418-431.

Carew TJ, Kandel ER (1973) Acquisition and retention of long-term habituation in Aplysia: correlation of behavioral and cellular processes. Science 182:1158-1160.

Castellucci V, Pinsker H, Kupfermann I, Kandel ER (1970) Neuronal mechanisms of habituation and dishabituation of the gill-withdrawal reflex in Aplysia. Science 167:1745-1748.

Courchesne E, Hillyard SA, Galambos R (1975) Stimulus novelty, task relevance and the visual evoked potential in man. Electroencephalogr Clin Neurophysiol 39:131-143.

Davis H, Osterhammel PA, Wier CC, Gjerdingen DB (1972) Slow vertex potentials: interactions among auditory, tactile, electric and visual stimuli. Electroencephalogr Clin Neurophysiol 33:537-545.

Forss N, Narici L, Hari R (2001) Sustained activation of the human SII cortices by stimulus trains. Neuroimage 13:497-501.

Fruhstorfer H (1971) Habituation and dishabituation of the human vertex response. Electroencephalogr Clin Neurophysiol 30:306-312.

Fruhstorfer H, Jarvilehto T, Soveri P (1969) Short-term habituation and dishabituation of the sensory evoked response in man. Acta Physiol Scand 76:14A-15A.

Fruhstorfer H, Soveri P, Jarvilehto T (1970) Short-term habituation of the auditory evoked response in man. Electroencephalogr Clin Neurophysiol 28:153-161.

Garcia-Larrea L, Frot M, Valeriani M (2003) Brain generators of laser-evoked potentials: from dipoles to functional significance. Neurophysiol Clin 33:279-292.

Greffrath W, Baumgartner U, Treede RD (2007) Peripheral and central components of habituation of heat pain perception and evoked potentials in humans. PAIN 132:301-311.

Hatem SM, Plaghki L, Mouraux A (2007) How response inhibition modulates nociceptive and non-nociceptive somatosensory brain-evoked potentials. Clin Neurophysiol 118:1503-1516.

Hu L, Mouraux A, Hu Y, Iannetti GD (2010) A novel approach for enhancing the signal-to-noise ratio and detecting automatically event-related potentials (ERPs) in single trials. Neuroimage 50:99-111.

Hu L, Valentini E, Zhang ZG, Liang M, Iannetti GD (2014a) The primary somatosensory cortex contributes to the latest part of the cortical response elicited by nociceptive somatosensory stimuli in humans. Neuroimage 84:383-393.

Hu L, Cai MM, Xiao P, Luo F, Iannetti GD (2014b) Human brain responses to concomitant stimulation of Adelta and C nociceptors. J Neurosci 34:11439-11451.

Hu L, Liang M, Mouraux A, Wise RG, Hu Y, Iannetti GD (2011) Taking into account latency, amplitude, and morphology: improved estimation of single-trial ERPs by wavelet filtering and multiple linear regression. J Neurophysiol 106:3216-3229.

553 Huang G, Xiao P, Hung YS, Iannetti GD, Zhang ZG, Hu L (2013) A novel approach to predict
554 subjective pain perception from single-trial laser-evoked potentials. Neuroimage 81:283-293.
555 Iannetti GD, Hughes NP, Lee MC, Mouraux A (2008) Determinants of laser-evoked EEG responses:
556 pain perception or stimulus saliency? J Neurophysiol 100:815-828.
557 Iannetti GD, Leandri M, Truini A, Zambreanu L, Cruccu G, Tracey I (2004) Adelta nociceptor
558 response to laser stimuli: selective effect of stimulus duration on skin temperature, brain
559 potentials and pain perception. Clin Neurophysiol 115:2629-2637.
560 Jasper H, Sharpless S (1956) Habituation of the arousal reaction. Brain 79:655-680.
561 Larsson LE (1956) The relation between the startle reaction and the non-specific EEG response to
562 sudden stimuli with a discussion on the mechanism of arousal. Electroencephalogr Clin
563 Neurophysiol 8:631-644.
564 Lee MC, Mouraux A, Iannetti GD (2009) Characterizing the cortical activity through which pain
565 emerges from nociception. J Neurosci 29:7909-7916.
566 Legrain V, Guerit JM, Bruyer R, Plaghki L (2002) Attentional modulation of the nociceptive processing
567 into the human brain: selective spatial attention, probability of stimulus occurrence, and target
568 detection effects on laser evoked potentials. PAIN 99:21-39.
569 Liang M, Mouraux A, Chan V, Blakemore C, Iannetti GD (2010) Functional characterisation of sensory
570 ERPs using probabilistic ICA: effect of stimulus modality and stimulus location. Clin
571 Neurophysiol 121:577-587.
572 Mancini F, Beaumont AL, Hu L, Haggard P, Iannetti GD (2015) Touch inhibits subcortical and cortical
573 nociceptive responses. PAIN 156:1936-1944.
574 Mancini F, Bauleo A, Cole J, Lui F, Porro CA, Haggard P, Iannetti GD (2014) Whole-body mapping of
575 spatial acuity for pain and touch. Ann Neurol 75:917-924.
576 Maris E, Oostenveld R (2007) Nonparametric statistical testing of EEG- and MEG-data. J Neurosci
577 Methods 164:177-190.
578 Moayedi M, Liang M, Sim AL, Hu L, Haggard P, Iannetti GD (2015) Laser-Evoked Vertex Potentials
579 Predict Defensive Motor Actions. Cereb Cortex.
580 Moayedi M, Di Stefano G, Stubbs MT, Djeugam B, Liang M, Iannetti GD (2016) Nociceptive-Evoked
581 Potentials Are Sensitive to Behaviorally Relevant Stimulus Displacements in Egocentric
582 Coordinates. eNeuro 3.
583 Mountcastle VB (2005) Neural mechanisms of somatic sensation. Cambridge, Massachusetts: Harvard
584 University press.
585 Mouraux A, Iannetti GD (2009) Nociceptive laser-evoked brain potentials do not reflect nociceptive-
586 specific neural activity. J Neurophysiol 101:3258-3269.
587 Mouraux A, Iannetti GD, Plaghki L (2010) Low intensity intra-epidermal electrical stimulation can
588 activate Adelta-nociceptors selectively. PAIN 150:199-207.
589 Mouraux A, De Paepe AL, Marot E, Plaghki L, Iannetti GD, Legrain V (2013) Unmasking the
590 obligatory components of nociceptive event-related brain potentials. J Neurophysiol 110:2312-
591 2324.
592 Ritter W, Vaughan HG, Jr., Costa LD (1968) Orienting and habituation to auditory stimuli: a study of
593 short term changes in average evoked responses. Electroencephalogr Clin Neurophysiol 25:550-
594 556.
595 Ronga I, Valentini E, Mouraux A, Iannetti GD (2013) Novelty is not enough: laser-evoked potentials
596 are determined by stimulus saliency, not absolute novelty. J Neurophysiol 109:692-701.
597 Snyder E, Hillyard SA (1976) Long-latency evoked potentials to irrelevant, deviant stimuli. Behav Biol
598 16:319-331.

599 Spiegel J, Hansen C, Treede RD (1996) Laser-evoked potentials after painful hand and foot stimulation
600 in humans: evidence for generation of the middle-latency component in the secondary
601 somatosensory cortex. Neurosci Lett 216:179-182.
602 Sutton S, Braren M, Zubin J, John ER (1965) Evoked-potential correlates of stimulus uncertainty.
603 Science 150:1187-1188.
604 Treede RD, Kief S, Holzer T, Bromm B (1988) Late somatosensory evoked cerebral potentials in
605 response to cutaneous heat stimuli. Electroencephalogr Clin Neurophysiol 70:429-441.
606 Valentini E, Torta DM, Mouraux A, Iannetti GD (2011) Dishabituation of laser-evoked EEG
607 responses: dissecting the effect of certain and uncertain changes in stimulus modality. J Cogn
608 Neurosci 23:2822-2837.
609 Valentini E, Hu L, Chakrabarti B, Hu Y, Aglioti SM, Iannetti GD (2012) The primary somatosensory
610 cortex largely contributes to the early part of the cortical response elicited by nociceptive
611 stimuli. Neuroimage 59:1571-1581.
612 Venkatesan L, Barlow SM, Popescu M, Popescu A (2014) Integrated approach for studying adaptation
613 mechanisms in the human somatosensory cortical network. Exp Brain Res 232:3545-3554.
614 Wang AL, Mouraux A, Liang M, Iannetti GD (2010) Stimulus novelty, and not neural refractoriness,
615 explains the repetition suppression of laser-evoked potentials. J Neurophysiol 104:2116-2124.
616 Wastell DG, Kleinman D (1980) Fast habituation of the late components of the visual evoked potential
617 in man. Physiol Behav 25:93-97.
618 Wessel JR, Aron AR (2013) Unexpected events induce motor slowing via a brain mechanism for
619 action-stopping with global suppressive effects. J Neurosci 33:18481-18491.
620

Table I. *Fitting results for different models of ERP habituation*

		Vertex wave				Lateralised wave	
		Aβ-N2	**Aβ-P2**	**Aδ-N2**	**Aδ-P2**	**Aβ-N1**	**Aδ-N1**
$y = a + \frac{b}{x}$	**AICc**	-5.216	-18.7	27.08	50.37	-100.80	-83.07
	Adjusted r^2	0.89	0.85	0.67	0.56	0.24	0.20
$y = a + \frac{b}{x^c}$	**AICc**	-25.49*	-26.12*	5.58*	27.76*	-102.70*	-92.66*
	Adjusted r^2	0.92*	0.87*	0.77*	0.71*	0.28*	0.33*
$y = a + e^{-bx}$	**AICc**	120.5	89.20	91.33	0.06	-83.89	-71.36
	Adjusted r^2	0.10	0.12	0.03	95.92	-0.01	0.03

The asterisk (*) detonates the winning model for each wave and modality (lowest AICc and highest adjusted r^2).

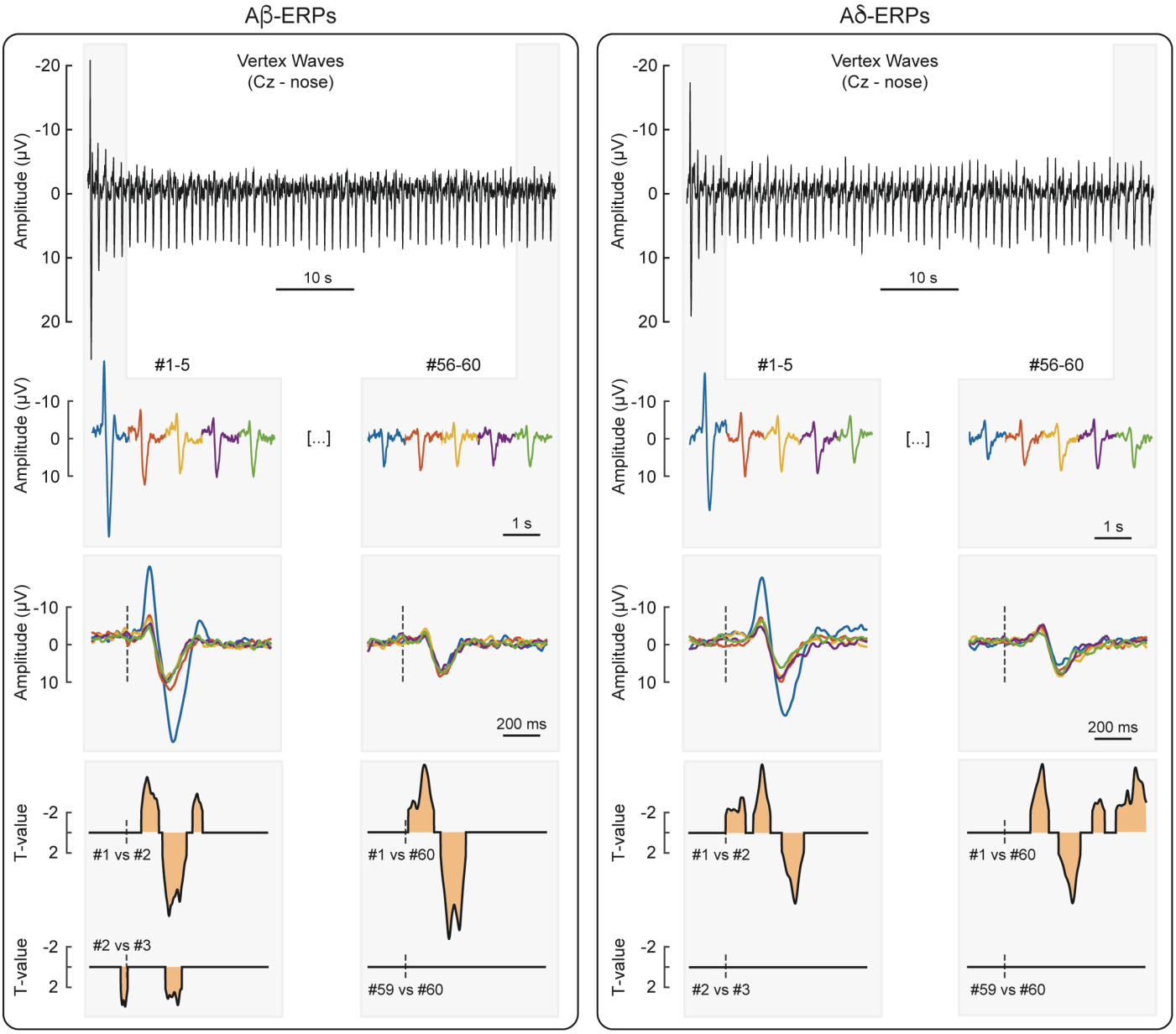
Aβ-ERPs
Aδ-ERPs
Vertex Waves
(Cz - nose)
Amplitude (µV)
-20
-10
0
10
20
10 s
#1-5
#56-60
[...]
1 s
200 ms
T-value
-2
2
#1 vs #2
#1 vs #60
#2 vs #3
#59 vs #60

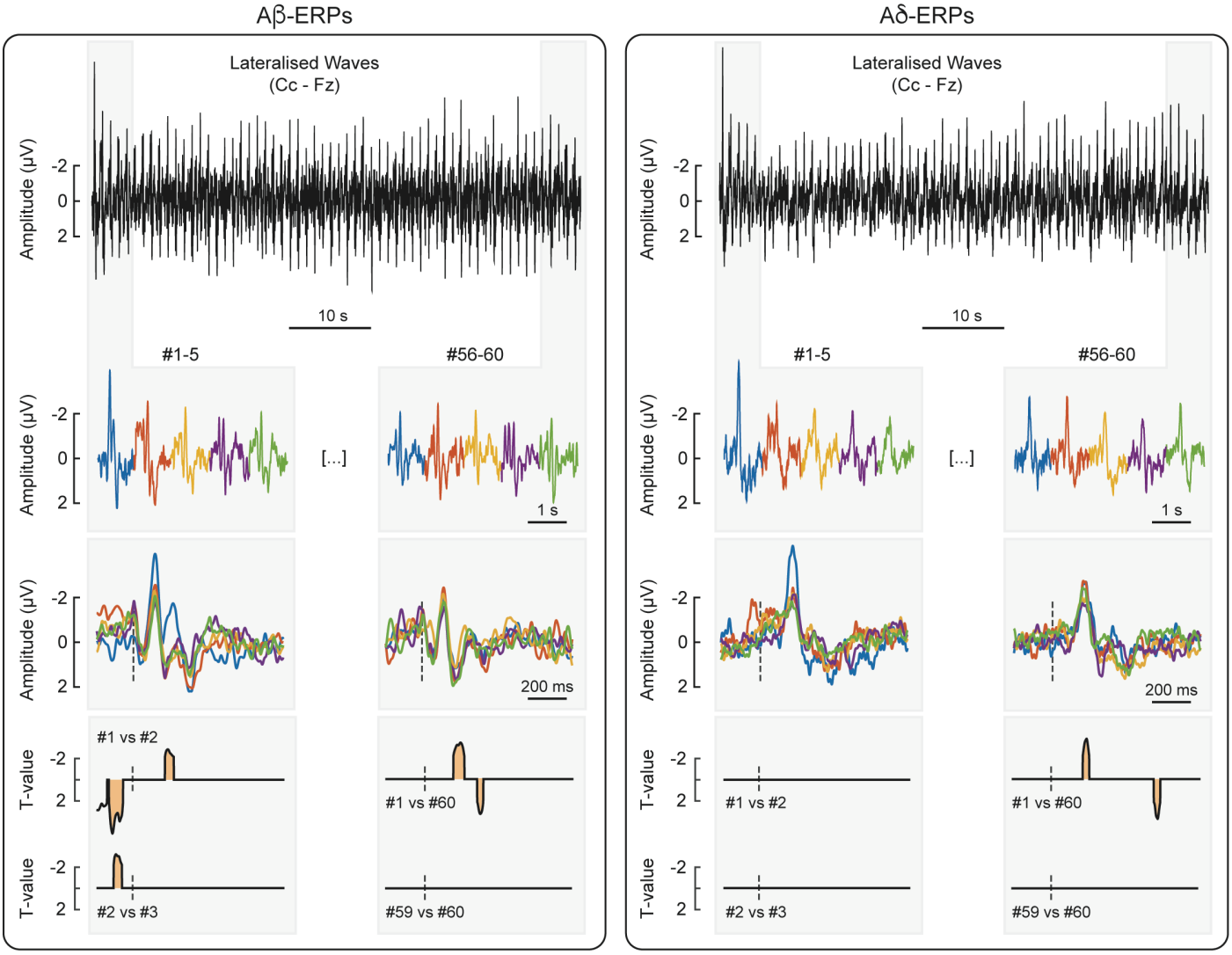
Aβ-ERPs
Aδ-ERPs
Lateralised Waves
(Cc - Fz)
Amplitude (µV)
-2
0
2
10 s
#1-5
#56-60
[...]
1 s
200 ms
T-value
#1 vs #2
#1 vs #60
#2 vs #3
#59 vs #60

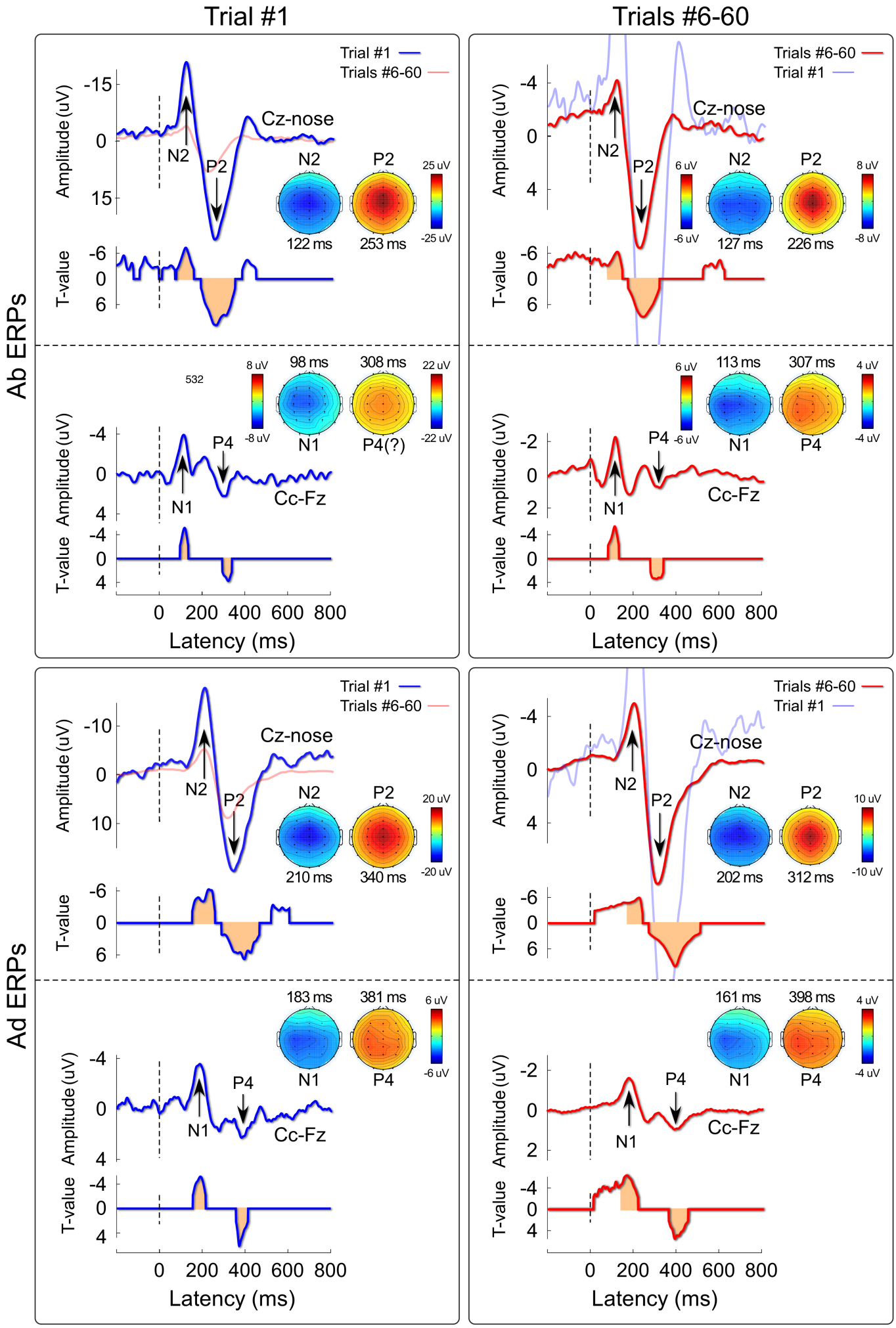
Trial #1
Trials #6-60
Ab ERPs
Ad ERPs
Trial #1
Trials #6-60
Cz-nose
N2
P2
N1
P4
Cc-Fz
P4(?)
Amplitude (uV)
T-value
Latency (ms)
0 200 400 600 800
122 ms
253 ms
127 ms
226 ms
98 ms
308 ms
113 ms
307 ms
210 ms
340 ms
202 ms
312 ms
183 ms
381 ms
161 ms
398 ms
532
25 uV
-25 uV
6 uV
-6 uV
8 uV
-8 uV
22 uV
-22 uV
4 uV
-4 uV
20 uV
-20 uV
10 uV
-10 uV

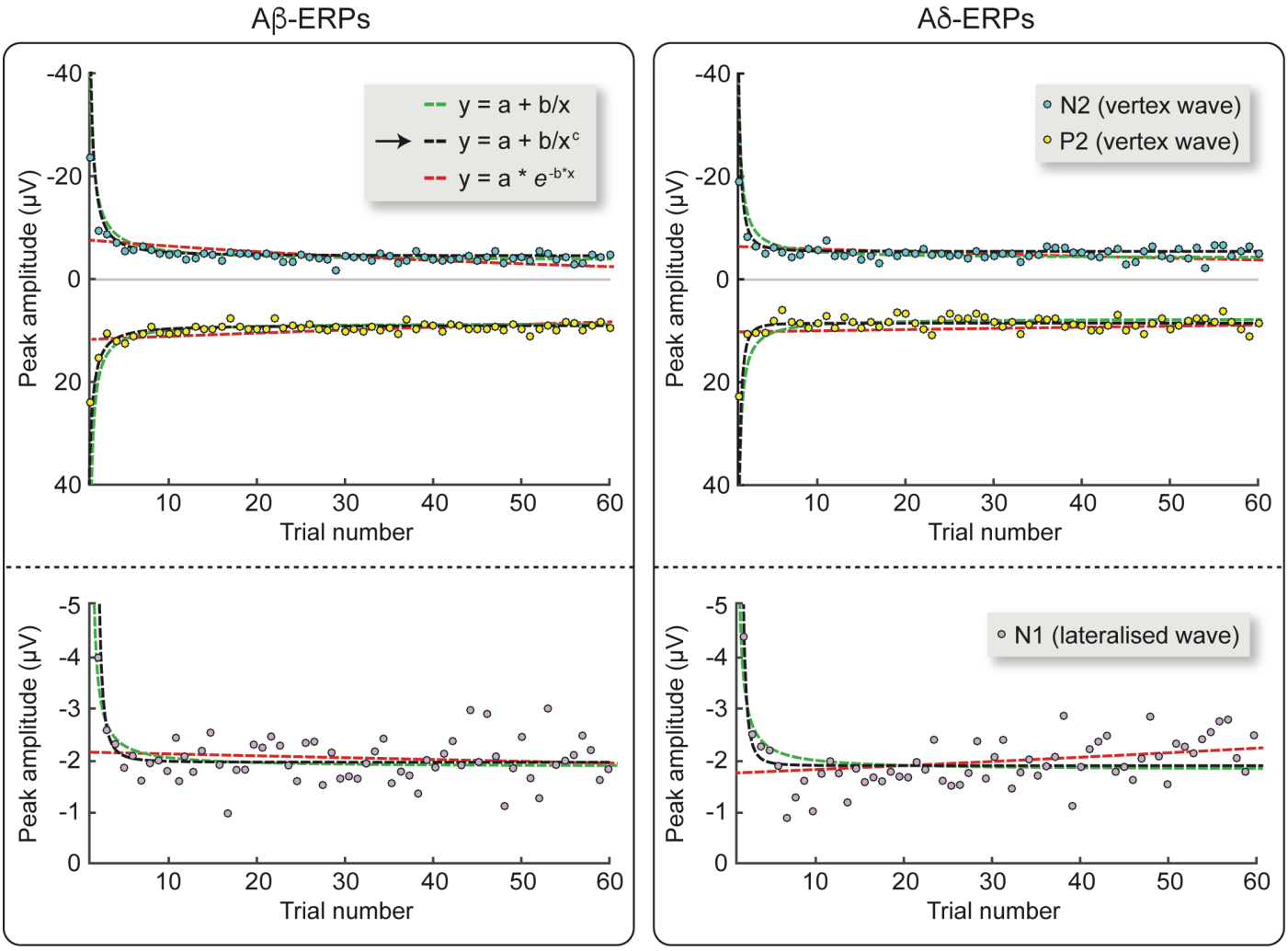
Aβ-ERPs
Aδ-ERPs
y = a + b/x
y = a + b/x^c
y = a * e^-b*x
N2 (vertex wave)
P2 (vertex wave)
N1 (lateralised wave)
Peak amplitude (µV)
Trial number
-40
-20
0
20
40
-5
-4
-3
-2
-1
10
20
30
40
50
60

Supplementary Results

Blind source separation using Probabilistic-ICA (pICA)

We decomposed non-habituated and habituated ERPs in functionally independent components, by performing a blind source separation with Independent Component Analysis (ICA) (Makeig et al., 1997) constrained to an effective estimate of the intrinsic dimensionality of the original data (probabilistic ICA, pICA) (Beckmann and Smith, 2004; Mouraux and Iannetti, 2009; Liang et al., 2010).

When applied to multi-channel EEG recordings, unconstrained ICA separates the signals recorded on the scalp into a linear combination of independent components (ICs), each having a fixed scalp topography and a maximally independent time course. When ICA is unconstrained, the total number of ICs equals the total number of recording electrodes. If the number of ICs differs greatly from the actual number of independent sources contributing to the signal, this may constitute a critical problem (Beckmann and Smith, 2004). Indeed, if the number of ICs is much larger than the number of sources, ICs containing spurious activity will appear because of overfitting. On the contrary, if the number of ICs is much smaller than the number of sources, valuable information will be lost due to under-fitting. The problem of overfitting could be particularly important when unconstrained ICA is applied to averaged ERP waveforms. Because the averaging procedure cancels out sources of activity unrelated to the stimulus (e.g. ongoing EEG activity, muscular activity and noise), the number of independent sources present in the average waveform may be far smaller than the number of independent sources present in the original EEG signal.

These fundamental limitations can be addressed using pICA, in which the number of ICs is constrained to an effective estimate of the number of independent sources contributing to the original data (Beckmann and Smith, 2004). The number of independent sources was estimated using a method based on maximum likelihoods, and operating on the eigenvalues of a Principal Component Analysis (Rajan and Rayner, 1997).

pICA was conducted on the signals averaged across subjects, and was performed separately, for each of the two sensory modalities, on the non-habituated ERP (trial #1) and on the habituated ERP (average of trials #6-60). pICA was also conducted on the concatenated non-habituated and habituated ERP, i.e. on the average ERP waveform from trial #1 concatenated to the average ERP waveform from trials #6-60. The functional decomposition of Aβ and Aδ ERPs are presented in Figures S1 and S2. These figures show the topographic distribution of each independent component (IC), ranked according to the percentage of explained variance, together with their contribution to the ERPs at channel Cz and to the EEG global field power (GFP).

Aβ-ERPs. pICA identified five ICs in the ERP elicited by stimulus 1 (Figure S1A), and five ICs in the ERP elicited by the average of stimuli 6-60 (Figure S1B).

In the ERP elicited by stimulus 1, IC #1 and #2 explained the majority of the P2 wave (GFP peak latencies: 241 and 293 ms), and were centrally distributed, with a maximum over the vertex

electrodes. IC #3 and #4 explained the majority of the N2 wave (peak latencies: 113 and 143 ms), although their distribution was not fully centred on the scalp vertex. IC #5 contributed to both the earliest and the latest part of the ERP time-course, and likely reflected lateralised responses (peak latencies: 67 and 347 ms). Accordingly, its scalp distribution was contralateral to the stimulated hand. Both the scalp distribution and the timecourse of these components match well previous blind source separation of ERPs elicited by intense and isolated somatosensory stimuli (Liang et al., 2010).

In the ERP elicited by stimuli 6-60, IC #1 explained the majority of the P2 wave (GFP peak latency: 238 ms), whereas IC #2 explained the majority of the N2 wave (peak latency: 135 ms). IC #3 isolated EEG activities contralateral to the stimulated hand, occurring in both early and late time windows of the signal (peak latencies: 112 and 389 ms). Therefore, the neural activity isolated by IC #3 are likely to correspond to the N1 and P4 waves of somatosensory ERPs.

To further assess whether the same components contributed to the non-habituated and habituated ERP waves, we performed a pICA on the concatenated ERP waveforms elicited by stimulus 1 and by the average of stimuli 6-60. This analysis identified five ICs (Figure S1C). IC #1 was symmetrically distributed over the vertex and explained the vast majority of the N2 wave in both the non-habituated and habituated response, as well as part of the P2 wave in the non-habituated ERP. IC #2 was also maximal over Cz, and contributed to the majority of the P2 wave in the response elicited by both stimulus 1 and stimuli 6-60. No single IC unequivocally isolated neural activities corresponding to the lateralised N1 and P4 waves shown in Figure 2.

Aδ-ERPs. Probabilistic ICA identified six ICs from the EEG responses to stimulus 1, and four ICs from the EEG responses to the average of stimuli 6-60 (Figure S2).

In the ERP elicited by stimulus 1, IC #1 and #2 had the typical topographical distribution of a vertex wave: IC #1 explained the majority of the P2 wave (GFP peak latency: 347 ms), and IC #2 explained the majority of the N2 wave (peak latency: 185 ms). IC #3 had a central-parietal distribution contralateral to the stimulated hand, and clearly reflected the late P4 wave observed in laser ERPs (peak latency: 423 ms) (Hu et al., 2014; Mancini et al., 2015). Probably because of the low signal-to-noise ratio consequent to the small number of stimulus repetitions, no IC unequivocally explained the early contralateral neural activity.

In the ERP elicited by stimuli 6-60, IC #1 was again centrally and symmetrically distributed and explained the majority of the P2 wave (peak latency: 307 ms). IC #2 had a contralateral central-parietal distribution contralateral to the stimulated hand, and explained the P4 wave (peak latency: 389 ms). ICs #3 had a maximal distribution over Cz and C3, and contributed to both the N1 and N2 waves (peak latency: 196 ms), possibly because of underfitting. IC #4 had a distribution contralateral to the stimulated hand and explained the early part of the N1 wave (peak latency: 138 ms).

pICA performed on the concatenated non-habituated and habituated ERP waves identified six ICs (Figure S2C). IC #1 and #2 were symmetrically distributed over the vertex. They explained the majority of the P2 wave (IC #1) and N2 wave (IC #2) in the response elicited by both

stimulus 1 and stimuli 6-60. IC #3 had a maximal distribution over Pz and P3, and explained the early N1 wave and part of the late P4 modality-specific waves, both in the non-habituated and habituated response. Finally, IC #4 had maximal distribution over C3, Cz, and C4, and explained a late positive wave in the response to both stimuli 1 and 6-60.

In conclusion, irrespectively of amplitude differences, the spatiotemporal pattern of the evoked brain activity was qualitatively similar not only for Aβ-ERPs and Aδ-ERPs (Treede et al., 1988), but also for the response elicited by stimulus 1 and stimuli 6-60.

Figure captions

Figure S1. *Functional decomposition of the Aβ-ERP elicited by the first stimulus (A, top-panel), by the average of stimuli 6-60 (B, middle panel), and of the concatenated Aβ-ERP elicited by stimulus 1 and 6-60 (C, bottom panel).* The top row of each panel shows the scalp topographies of the Independent Components (ICs), identified by the probabilistic Independent Component Analysis (pICA). The middle row of each panel shows the signals obtained by back-projecting each IC (thick colored waveforms) onto channel Cz. The original ERP waveforms at Cz is shown as a thin and grey line. The bottom row of each panel shows the contribution of each IC to the global field power.

Figure S2. *Functional decomposition of the Aδ-ERP elicited by the first stimulus (A, top-panel), by the average of stimuli 6-60 (B, middle panel), and of the concatenated Aδ-ERP elicited by stimulus 1 and 6-60 (C, bottom panel).* The top row of each panel shows the scalp topographies of the Independent Components (ICs), identified by pICA. The middle row of each panel shows the signals obtained by back-projecting each IC (thick colored waveforms) onto channel Cz. The original ERP waveforms at Cz is shown as a thin and grey line. The bottom row of each panel shows the contribution of each IC to the global field power.

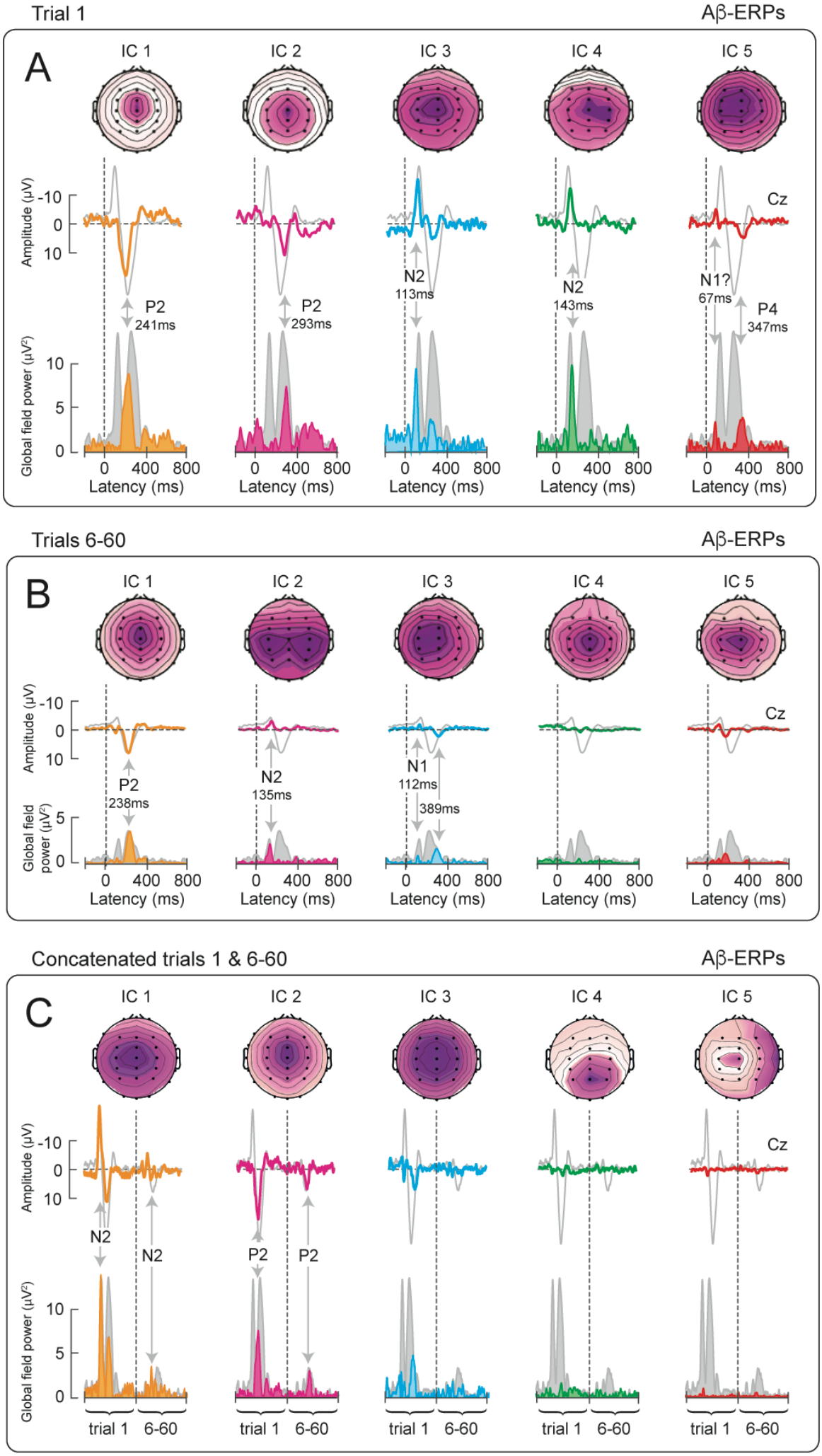
Trial 1
Aβ-ERPs
A
IC 1
IC 2
IC 3
IC 4
IC 5
Amplitude (μV)
-10
0
10
Cz
P2
241ms
P2
293ms
N2
113ms
N2
143ms
N1?
67ms
P4
347ms
Global field power (μV²)
10
5
0
0 400 800
Latency (ms)
Trials 6-60
Aβ-ERPs
B
P2
238ms
N2
135ms
N1
112ms
389ms
Concatenated trials 1 & 6-60
Aβ-ERPs
C
N2
N2
P2
P2
trial 1
6-60

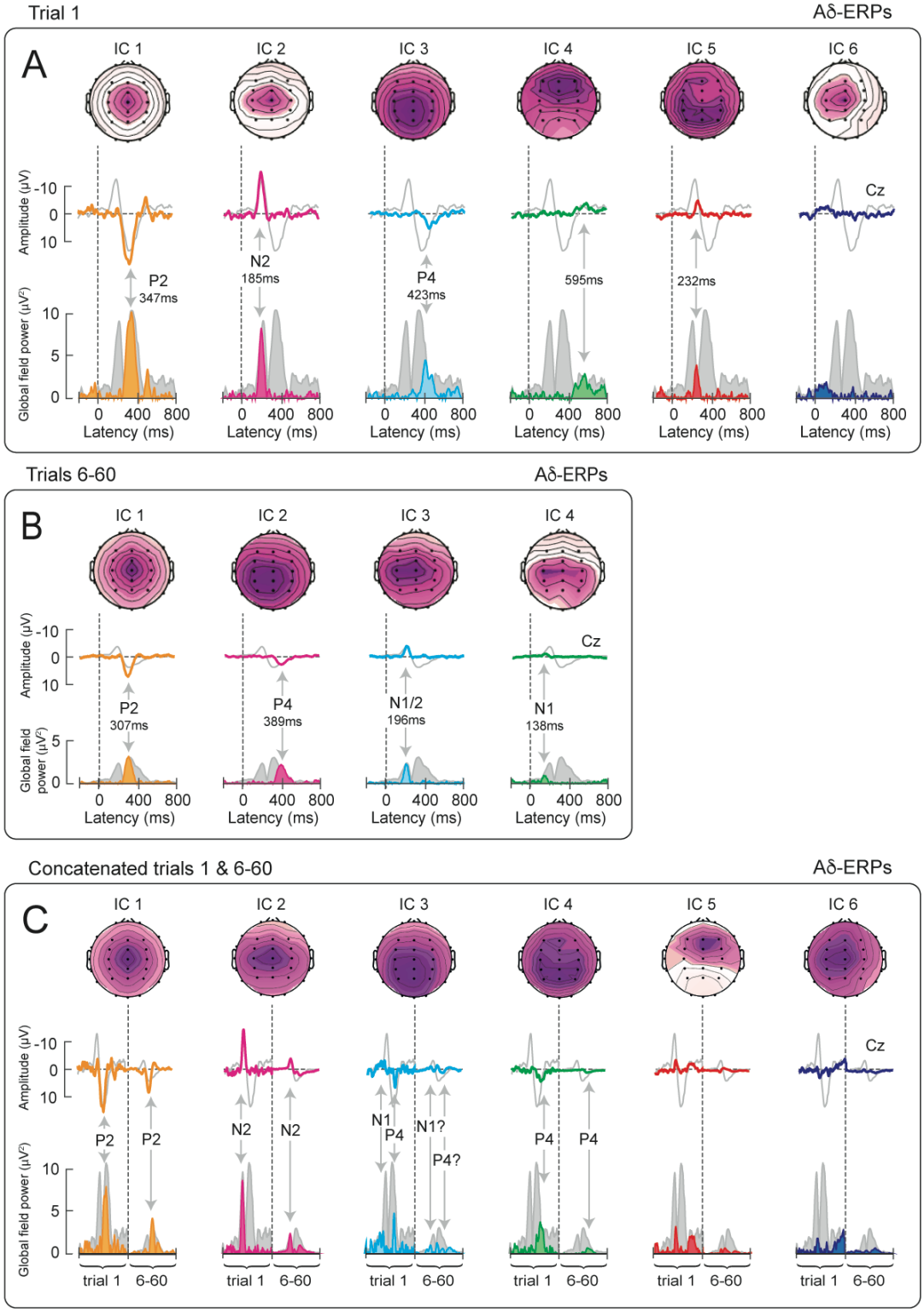
Trial 1
Aδ-ERPs
A
IC 1
IC 2
IC 3
IC 4
IC 5
IC 6
Amplitude (µV)
-10
0
10
Cz
P2
347ms
N2
185ms
P4
423ms
595ms
232ms
Global field power (µV²)
10
5
0
0 400 800
Latency (ms)
Trials 6-60
Aδ-ERPs
B
IC 1
IC 2
IC 3
IC 4
Amplitude (µV)
-10
0
10
Cz
P2
307ms
P4
389ms
N1/2
196ms
N1
138ms
Global field power (µV²)
5
0
0 400 800
Latency (ms)
Concatenated trials 1 & 6-60
Aδ-ERPs
C
IC 1
IC 2
IC 3
IC 4
IC 5
IC 6
Amplitude (µV)
-10
0
10
Cz
P2
P2
N2
N2
N1
P4
N1?
P4?
P4
P4
Global field power (µV²)
10
5
0
trial 1
6-60